

Preparation of the Ordered Spherical Ru-RuO₂ and Electrocatalysis toward Chlorine Evolution Reaction

Ju Wang, Conghui Zhai, Hanruo Chen, Ning Cong, Lingjun Tan, Hua Fang, Xiaorong Zhou, Zhandong Ren and Yuchan Zhu*

School of Chemical and Environmental Engineering, Wuhan Polytechnic University, Wuhan, 430023, P. R. China.

*E-mail: zhuyuchan@163.com

Received: 4 July 2019 / Accepted: 20 August 2019 / Published: 7 October 2019

Chlorine evolution reaction (CER) is a very important electrochemical reaction process in modern electrochemical industry. To develop an efficient CER electrode, not only the active components but also the morphology of the electrode should be considered. In this work, the ordered spherical Ru-RuO₂ electrode was prepared by hydrothermal reaction for improving the CER activity. X-ray photoelectron spectroscopy (XPS), scanning electron microscopy (SEM) and X-ray diffraction (XRD) characterizations were employed to analyze the electrode structures. Compared with RuO₂ electrode prepared by Adams method, the CER activity of Ru-RuO₂ electrode is obviously improved. The improvement of activity should be attributed to the change of electronic structure and the ordered structure of electrode surface. The prepared Ru-RuO₂ particles are spherical and evenly distributed, thus showing an orderly morphology. Such an unified structure can be conducive to the diffusion of Cl₂. The diffraction peak of (101) crystal plane of Ru-RuO₂ electrode has slightly positive shifted of 0.4°. It indicates that the lattice of RuO₂ on the outside surface of Ru-RuO₂ has been compressed to a certain extent, which may reduce the adsorption energy of Cl and accelerate the rate of chlorine desorption process.

Keywords: Chlorine evolution reaction, Ru-RuO₂, ordered structure, electronic structure

1. INTRODUCTION

Electrochemical chlorine evolution reaction (CER) is very important in modern electrochemical industry [1-7]. Around the world, large amounts of chlorine are used to produce a wide variety of chemicals [8]. The electrochemical process of CER is $2\text{Cl}^- - 2\text{e} = \text{Cl}_2$ ($E^\circ = 1.36$ V vs. SHE, anode). The most important factor affecting CER activity is electrode material. So far, the state-of-the-art electrodes for CER are dimensionally stable anodes (DSAs) based on Ru(Ir)-based composite oxide electrodes [9-15]. The electrocatalytic properties of RuO₂ present a lower oxygen/metal atomic fraction, a more

positive surface charge, lower binding energy, and more hydrophilic properties than IrO₂, which makes it more reactive [16]. In addition, many researches focus on multicomponent Ru and Ir composite oxides to further improve the CER activity, such as RuTi [17-24], RuSn [25-26], RuNi [27], IrTa [28], IrTi [29], RuIrTi [30], RuIrSn [31] and RuTiCeNb [32] composite oxides. In recent years, the use of the density functional theory (DFT) calculation analysis to guide the design and development of electrode materials is also an important aspect [33-38]. The CER activity of electrode materials can be predicted by analysing the relationship between the electronic properties of metal oxide electrode and hydrogen adsorption energy.

However, "bubble shielding effect", that is, the blocking effect of adsorption of Cl₂ bubbles on the electrode surface [39-40], has not received much attention. If a large number of Cl₂ bubbles generated by electrolysis cannot leave the electrode surface in time, it will seriously hinder electrolyte diffusion and increase ohmic drop. The "bubble shielding effect" can be minimized by modifying the surface morphology of electrodes to improve the surface hydrophobicity [17]. Moreover, constructing electrode surface with ordered structure is also an important method to improve "bubble shielding effect" [18, 25, 41]. Therefore, the development of efficient CER electrode should consider not only the active components but also the morphology of electrode surfaces. In this work, the ordered spherical Ru-RuO₂ electrode by hydrothermal method for improving the CER activity. XPS, SEM and XRD characterizations were employed to analyze the electrode structures. Compared with common RuO₂ electrode, the CER activity is obviously improved. The improvement of activity should be attributed to the change of electronic structure and the orderly electrode structure.

2. EXPERIMENTAL SETUP

2.1 Chemicals and materials

Ruthenium(III) chloride (RuCl₃·3H₂O), sodium nitrate (NaNO₃), sodium chloride (NaCl), ethanol (C₂H₅OH), isopropanol (C₃H₇OH), n-butyl alcohol (C₄H₉OH) and oxalic acid (H₂C₂O₄) were purchased from Sinopharm Chemical Reagent Co., Ltd., Shanghai, China. All reagents were analytical reagents and were not further purified. Argon gas (99.999%) in the cylinder was purchased from Wuhan Ming-Hui Company.

2.2 Ru-RuO₂ preparation

RuCl₃·3H₂O solid was dissolved in n-butyl alcohol solution with the Ru³⁺ concentration 0.065 mol L⁻¹. Then 80 ml of the solution was transferred to a stainless steel autoclave lined with Teflon with a filling degree of about 80%. The hydrothermal reaction temperature is controlled at 180 °C and the reaction time is 2h. After cooling to room temperature, the sample is taken out of the autoclave and washed alternately with anhydrous ethanol and high-purity water. The samples were dried at 100 °C and calcined at 400 °C for 4h in muffle furnace to obtain the Ru-RuO₂ catalyst.

2.3 RuO₂ preparation

NaNO₃ powder (0.442g) was added to 0.2 mol L⁻¹ RuCl₃ isopropanol solution (20 mL). The stirring is continuously carried out at 75 °C until the solution becomes pasty. The mixture was then put into a porcelain crucible and fed into a muffle furnace. Raise the temperature to 400 °C at a rate of 5 °C min⁻¹ and keep it for 30 minutes. After the muffle furnace was cooled to room temperature, the sample was taken out and washed clean. The supernatant was detected by 0.01mol L⁻¹ AgNO₃ solution until there was no Cl⁻. The sample was dried to obtain RuO₂ powder.

2.4 Electrode preparation

Ti plate was cut into a size of 1 cm × 3 cm as substrate. Then ultrasonic cleaning is carried out in acetone solution, aqueous solution and ethanol solution for 10 min respectively to remove oil stains on the surface of Ti plate. Then, Ti plate was pretreated with 10% H₂C₂O₄ at 96 °C for 2 h to obtain TiH surface with uniform roughness and gray color. Meanwhile, 0.05wt % nafion-ethanol solution was added to the 2.5mg catalyst and dispersed by ultrasound to get catalyst dispersion solution. 50 μL of the prepared catalyst dispersion solution is dropped in a 1 cm × 1 cm area on the Ti plate with loading 0.125 mg cm⁻². The electrode surface is coated with epoxy resin except for the working area of 1 cm × 1 cm.

2.5 Material characterization

X-ray diffraction (XRD) was carried out on the XRD-7000 instrument (Shimadzu, Japan, Cu Ka, 40 kV and 30 mA). Scanning electron microscopy (SEM) was used to analyze the electrode morphology with S-3000N apparatus (Hitachi, Japan). The electron properties of the electrode were characterized by ESCLAB 250Xi X-ray photoelectron spectrometer (XPS, Thermo Scientific, America). XPS Peak41 software was used to fit and analyze energy spectrum data.

2.6 Electrochemical measurements

Electrochemical tests were performed on an electrochemical workstation (CHI 760D) in a three-electrode electrolytic cell with 0.5 M H₂SO₄ solution. The working electrode, the counter electrode and the reference electrode are Ru-RuO₂ (RuO₂), carbon paper and mercury sulfite electrode (Hg/Hg₂SO₄/0.1 M K₂SO₄) respectively. In the range of 0-1.4 V, Cyclic voltammetry (CV) scanning was performed at the speed of 20 mV s⁻¹ to characterize the electrochemical properties of the electrode. The double-layer capacitance (C_d) test is carried out at different scanning speeds in the range of 0.3-0.4 V. Electrochemical chlorine evolution activity is obtained by linear sweep voltammetry (LSV) at a scanning speed of 5 mV s⁻¹ in the range of 1.10 - 1.65 V, with NaCl concentration of 4.0 M and pH=1.0. The electrochemical test was repeated three times.

3. RESULTS AND DISCUSSION

Fig. 1a is SEM image of Ru-RuO₂ prepared by hydrothermal method. The prepared Ru-RuO₂ particles are uniform in shape, forming an ordered structure. Ru-RuO₂ particles have a regular spherical structure with a very smooth surface and a particle size in the range of 400-600 nm. The formation of large particle size is due to the fact that the high pressure and high temperature conditions are conducive to particle agglomeration, accelerating nucleation and crystallization growth, and gradually forming an ordered spherical arrangement structure in the hydrothermal process. Such an orderly and unified structure would make the catalyst acquire excellent electrocatalytic activity for chlorine evolution. SEM image of RuO₂ prepared by Adams method is shown in Fig. 1b, which have irregular shapes and large difference in particle sizes. The size of small particles is less than 50 nm, while the size of large aggregate particles can reach 800 nm. Next, Figs. 1c and 1e have displayed the morphology of Ru-RuO₂ coated on the Ti substrate (Ru-RuO₂ electrode). Before coating, Ti plate was treated with oxalic acid to form a porous surface. The morphology of spherical Ru-RuO₂ did not change during the coating process, and its spherical particles were clearly visible in the SEM figures. Moreover, they are evenly distributed on the surface of Ti plate. For RuO₂ electrode, the morphology and distribution on the Ti plate are slightly different from that of Ru-RuO₂ electrode. The fine RuO₂ particles are rarely found in Figs. 1d and 1f, which may be filled into the interior of large holes on the surface of Ti plate. In addition, consistent with Fig. 1b, some large particles can still be observed in Fig. 1d and 1f.

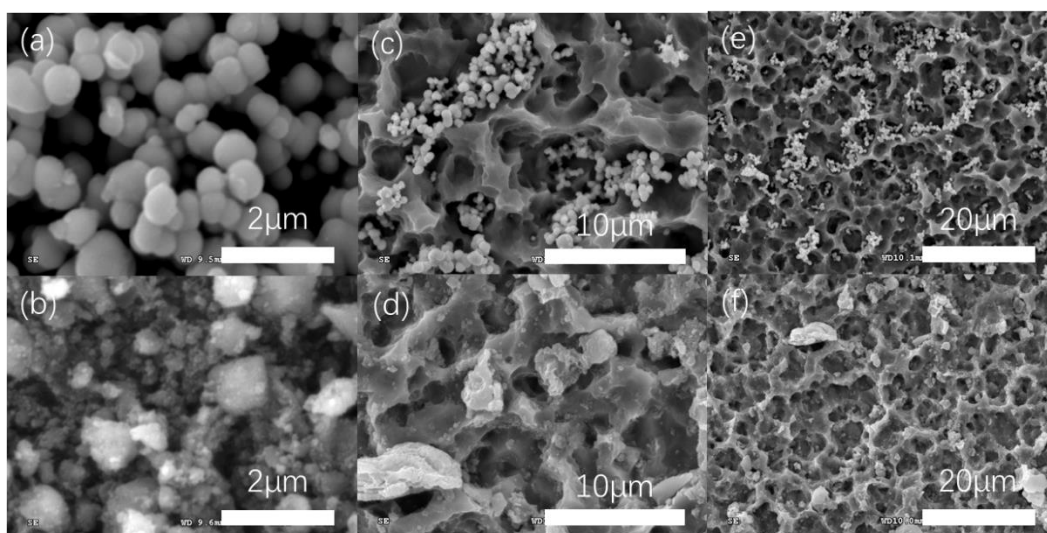


Figure 1. Morphologies of Ru-RuO₂ (a, c, e) and RuO₂ (b, d, f) electrodes.

The crystal structure of Ru-RuO₂ was analyzed by XRD in Fig. 2a. The diffraction peaks at 38.4°, 42.1°, 43.9°, 58.4°, 69.5°, 78.5°, 82.6°, 84.8° and 86.0° respectively correspond to the (100), (002), (101), (102), (110), (103), (200), (112) and (201) crystal planes of Ru by comparing Ru-PDF06-0663 [43]. It is due to the reduction of n-butanol forming a reduced metal Ru in the hydrothermal reaction process. According to RuO₂-PDF43-1027, the diffraction peaks at 28.1°, 35.6° and 54.4° correspond to the (110), (101) and (211) crystal planes, respectively [22]. It is caused by high temperature thermal

oxidation in the air in the subsequent step of hydrothermal reaction. Since the thermal oxidation reaction process is after the hydrothermal synthesis, the formed Ru-RuO₂ catalyst should be RuO₂ in the outer layer and Ru in the inner layer. In addition, compared with RuO₂ prepared by Adams method, the diffraction peak of (101) crystal plane of Ru-RuO₂ electrode has slightly positive shifted of 0.4° in Fig. 2b. It indicates that the lattice of RuO₂ on the outside surface of Ru-RuO₂ has been compressed to a certain extent, which may be due to the lattice deformation of Ru metal on the outer layer of RuO₂.

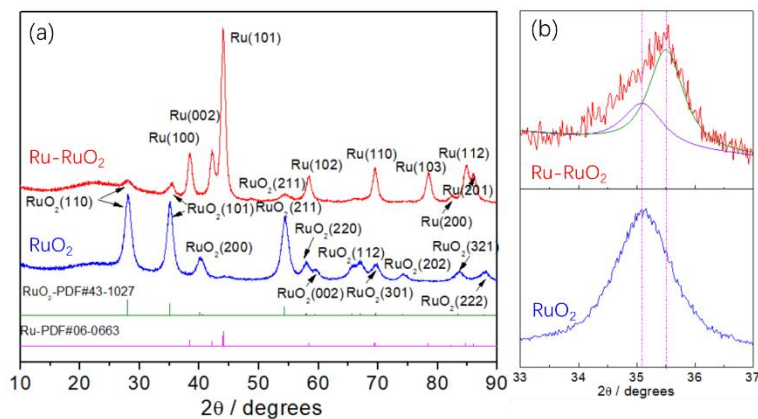


Figure 2. X-ray diffraction curves for Ru-RuO₂ and RuO₂ electrodes in 10-90° (a). Detailed comparison of (101) crystal surfaces of Ru-RuO₂ and RuO₂ electrodes in 32-37° (b).

Fig. 3 are high-resolution XPS spectra of Ru-RuO₂ electrode. As can be seen from Fig. 3a, the peaks at 284.6 eV and 280.7 eV correspond to the spin splitting peaks of 3d_{3/2} and 3d_{5/2} orbits of Ru⁴⁺ [42]. The peaks located at 286.7 eV and 282.1 eV are satellite peaks belonging to the Ru⁴⁺ 3d_{3/2} and Ru⁴⁺ 3d_{5/2} orbits. The peak of 529.4 eV, 531.1 eV Ru and 533.3 eV in Fig. 3b is attributed to O 1s orbital in O²⁻, OH⁻ and H₂O, respectively. In addition, the vibration peak of C 1s orbital is located at 284.8 eV in Fig. 3a. The analysis result has indicated that the outside surface of Ru-RuO₂ electrocatalyst is indeed in oxidation state of RuO₂, not in reduction state of Ru.

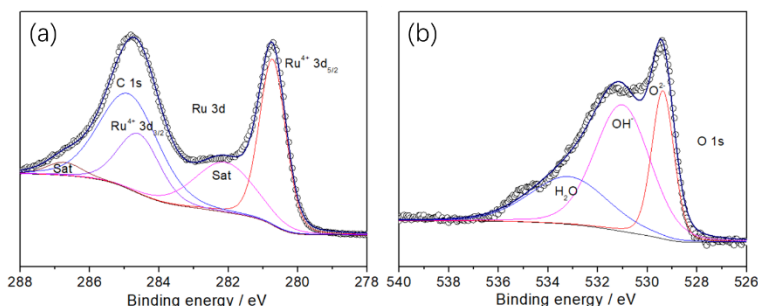


Figure 3. High-resolution XPS spectra of the Ru 3d and O 1s orbitals of Ru-RuO₂ electrode.

Electrochemical cyclic voltammetry curves (CVs) were used to characterize the electrochemical characteristics of Ru-RuO₂ and RuO₂ electrodes. Fig. 4a is a typical CV graph of RuO₂ electrode in acidic medium [18, 31]. In the range of 0-0.4 V (hydrogen region), the obvious hydrogen under-potential deposition (H-UPD) current can be seen. In the range of 0.4-1.35 V, there are three pairs of obvious

redox peak positions at (a1, a1'), (a2, a2') and (a3, a3'), which respectively correspond to $\text{Ru}^{2+}/\text{Ru}^{3+}$, $\text{Ru}^{3+}/\text{Ru}^{4+}$, $\text{Ru}^{4+}/\text{Ru}^{6+}$ [9, 15, 21, 32]. Moreover, the electrode surface may be further oxidized to Ru^{8+} at high potential (> 1.35 V), which is accompanied by oxygen evolution reaction on the surface. Fig. 4b is a CV graph of Ru-RuO₂ electrode, which is obviously different from that of RuO₂ electrode. In the high potential region, except the redox peak of $\text{Ru}^{2+}/\text{Ru}^{3+}$ (tiny peak at (a1, a1')), the redox peaks at other potentials are no longer obvious. It may be related to the low content of RuO₂ in the surface of Ru-RuO₂ electrode. In addition, the CV curve of Ru-RuO₂ electrode is obviously different from that of RuO₂ electrode in the hydrogen region. An obvious H-UPD current peak at 0.07 V and a certain hydrogen evolution current at 0.03 V are found in the CV curve of Ru-RuO₂ electrode.

Electrochemical surface area (ESA) is an important factor affecting electrocatalytic activity, so the ESA of Ru-RuO₂ electrode was further investigated. It is a common method to estimate the ESAs of electrodes by using double-layer capacitance (C_d) [16, 17, 21]. From the CV diagram, it can be seen that there is no obvious oxidation-reduction current between 0.3 and 0.4 V, indicating that this range is a double-layer region. In this interval, CV scanning was performed at different scan rate from 1 to 100 mV s^{-1} in Fig. 4e and 4f. The relationship between scan rate and double-layer current was obtained in Fig. 4b and 4d. And the C_d and ESA of two kinds of electrodes were then calculated. The ESA of Ru-RuO₂ electrode is 76.5 cm^2 , while the ESA of RuO₂ electrode is 94.3 cm^2 .

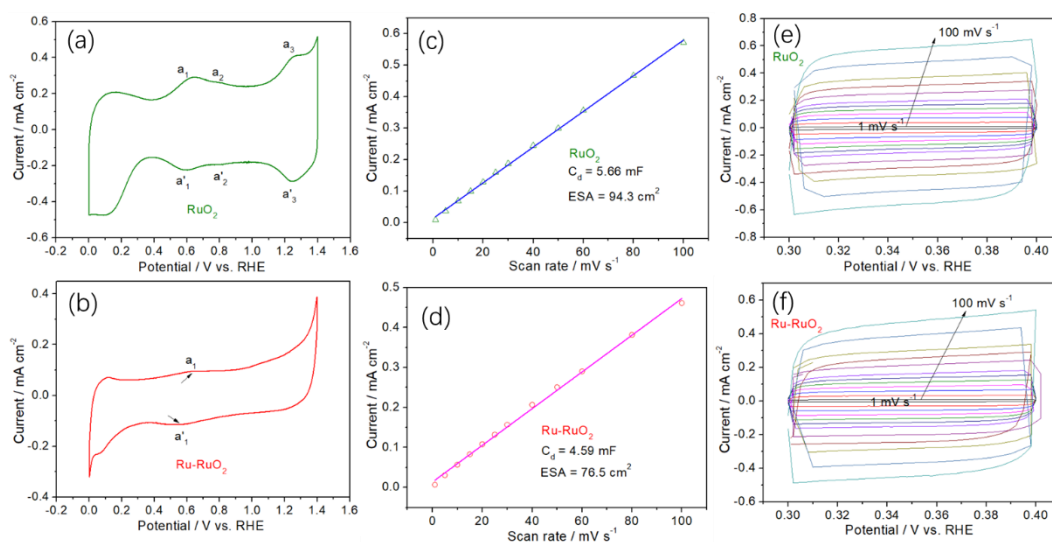


Figure 4. Cyclic voltammograms (CVs) and electrochemical surface areas (ESAs) of RuO₂ (a, c) and Ru-RuO₂ electrodes (b, d). Double-layer diagram of RuO₂ (e) and Ru-RuO₂ (f) at different scan rate from 1 to 100 mV s^{-1} .

Next, the electrochemical activity of CER was further observed using linear sweep voltammetry. Fig. 5a has displayed the apparent current density in the range of $-0.2 - 0.2$ V. The CER activity of Ru-RuO₂ electrode is significantly better than that of RuO₂ electrode. At a potential of 1.6 V, the apparent current density of Ru-RuO₂ electrode is 0.066 A cm^{-2} , while that of RuO₂ electrode is only 0.044 A cm^{-2} . The gap between them is 1.5 times. Then the apparent current was further normalized by its ESA to obtain the specific activity in Fig. 5b. At 1.6 V, the specific activity of RuO₂ electrode is only 0.46 mA cm^{-2} , while that of Ru-RuO₂ electrode is increased to 0.84 A cm^{-2} by 1.8 times.

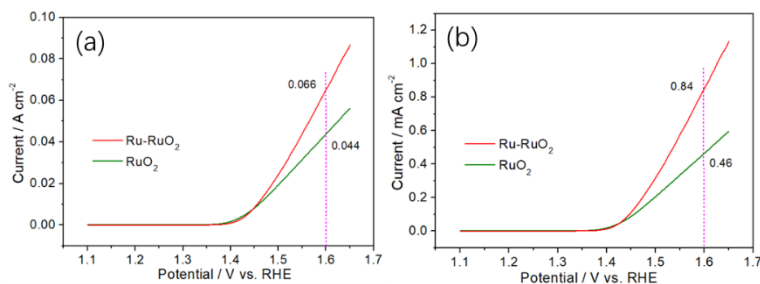


Figure 5. Apparent activity (a) and specific activity (b) of chlorine evolution reaction (CER) of Ru-RuO₂ and RuO₂ electrodes.

Some apparent activities of CER reported in the literature are listed in Table 1. Catalyst composition, catalyst loading, preparation method, NaCl concentration and pH value all have effects on apparent activity. Among them, the CER activity of RuO₂-TiO₂ composite is generally higher than that of RuO₂. The activity of CER was significantly increased with the increase of catalyst loading and NaCl concentration. Although the CER activity of Ru-RuO₂ in this article are not significantly higher than those in the literature [18, 20], the Ru-RuO₂ loading is very low (1/10 of the load in the literature), thus greatly improving the mass specific activity of the precious metal Ru (3-10 times higher than that in the literature).

Table 1. Comparing different electrocatalysts for chlorine evolution reaction

Catalyst	Preparation method	Loading (mg cm ⁻²)	Electrolyte solution	CER current (mA cm ⁻²) vs. RHE	Ref.
Si/BDD/Ru O ₂	Sol-gel	0.035	2M NaCl pH = 2	~2.8 @ 1.60 V	[11]
RuO ₂ /Ti	Thermal decomposition	---	5 M NaCl, pH = 2	50-60 @ 1.60 V	[16]
RuO ₂ /TiO ₂	Thermal decomposition	---	4 M NaCl, pH = 3	~0.35 @ 1.50 V	[24]
RuO ₂ /Ti	Microwave-solvothermal	0.70	0.1 M NaCl	~1.5 @ 1.60 V	[43]
RuO ₂ -TiO ₂ /Ti	Sol-gel or Thermal decomposition	2.00	5 M NaCl, pH = 2	8-10 @ 1.50 V	[9]
RuO ₂ -TiO ₂ /Ti	Thermal decomposition	---	Sat. NaCl, pH = 2	15-20 @ 1.50 V	[17]
TiO ₂ -RuO ₂ /Ti	Thermal decomposition	1.20	5 M NaCl, pH = 3	~160 @ 1.60 V	[18]
Ru _{0.3} Ti _{0.7} O ₂	Commercial	1.21	3.5 M NaCl,	65-75 @ 1.60 V	[20]

Ti–Ru–Ir ternary oxide	Commercial	---	pH = 3 4M NaCl, pH = 2	~45 @ 1.60 V	[30]
Ru–RuO ₂	Hydrothermal method	0.125	4M NaCl, pH = 1	66 @ 1.60 V 24 @ 1.50 V	This work

It is generally believed that the reaction rate of CER is influenced by the external surface area of electrode material, and has nothing to do with the internal surface area of electrode. Therefore, in addition to the total ESA (Fig. 4), it is necessary to investigate the external surface charge (q_{out}) and the internal surface charge (q_{in}) of Ru–RuO₂ electrode (Fig. 6) [4, 10, 18, 31]. From Figs. 6a and 6b, the total surface charge (q_{tot}), q_{out} and q_{in} ($q_{in} = q_{tot} - q_{out}$) can be calculated to be 1.32 mC, 0.81 mC and 0.51 mC respectively. The q_{tot} , q_{out} and q_{in} of RuO₂ electrode is 1.52 mC, 1.00 mC and 0.52 mC, respectively. The q_{out} of RuO₂ electrode is higher than that of Ru–RuO₂ electrode, which is consistent with the results of their ESAs. Therefore, the increase of CER activity of Ru–RuO₂ electrode is not caused by the change of surface charge.

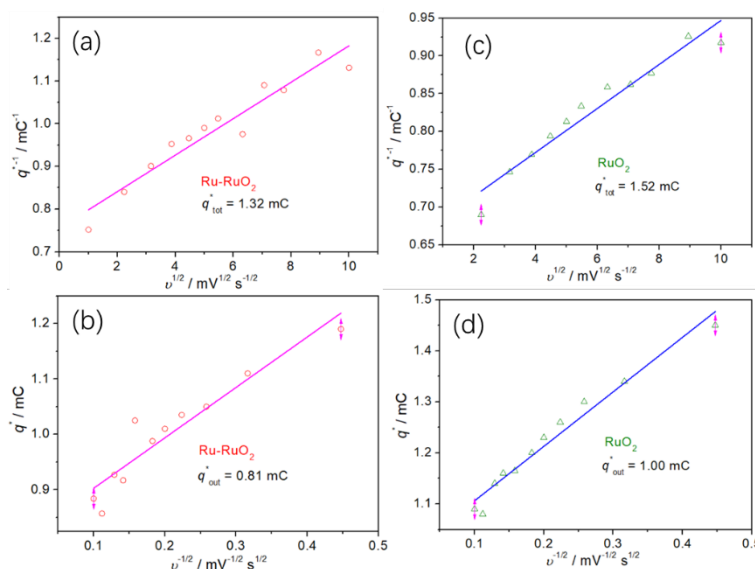
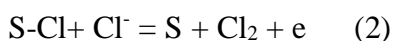
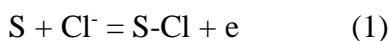


Figure 6. The total surface charge (q_{tot}) and the external surface charge (q_{out}) of RuO₂ (a, c) and Ru–RuO₂ electrodes (b, d).

Most literatures believe that the process of CER on RuO₂ electrode is the Volmer–Heyrovsky mechanism [11, 14, 17, 28, 33, 36, 38]. When formula 1 and 2 is the rate determining step, the Tafel slope is 120 and 40 mV dec⁻¹, respectively. (S represents the electrode surface)



Then, the CER mechanism was further analyzed by Tafel slope. As can be seen from Fig. 7, the Tafel slope of Ru-RuO₂ electrode is 36.0 mV dec⁻¹, indicating that the CER reaction rate is controlled by chlorine desorption process (Step 2) [33]. In order to accelerate the rate of step 2, the adsorption energy of Cl should be reduced. From the previous XRD characterization, it can be seen that the lattice of RuO₂ on the outside surface of Ru-RuO₂ electrode has shrunk to a certain extent, which may reduce the adsorption energy (More details will be studied in subsequent experiments). On the other hand, the diffusion rate of Cl₂ in step 2 should be accelerated with the ordered structure of Ru-RuO₂ electrode, which would be conducive to the enhancement of CER activity.

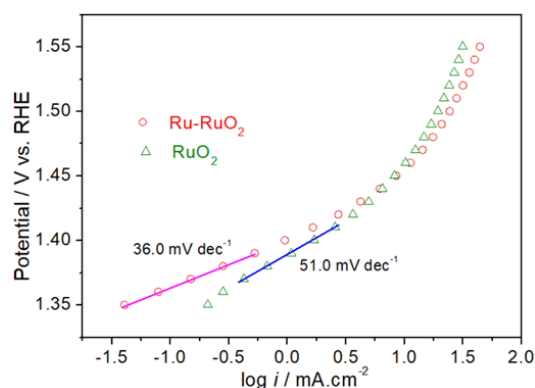


Figure 7. The Tafel slopes of chlorine evolution reaction (CER) of Ru-RuO₂ and RuO₂ electrodes.

4. CONCLUSIONS

In this work, the ordered spherical Ru-RuO₂ electrode by hydrothermal method was prepared for improving the CER activity. The enhancement of activity should be attributed to the change of electronic structure and the orderly electrode surface structure. The prepared Ru-RuO₂ particles are spherical in shape and evenly distribution, forming a uniform and orderly structure. Such an orderly and unified structure can be conducive to the diffusion of Cl₂. Compared with RuO₂ prepared by Adams method, the diffraction peak of (101) crystal plane of Ru-RuO₂ electrode has slightly positive shifted of 0.4°. It indicates that the lattice of RuO₂ on the surface of Ru-RuO₂ has been compressed to a certain extent, which may reduce the adsorption energy of Cl and accelerate the rate of chlorine desorption process.

ACKNOWLEDGMENTS

The authors would like to acknowledge financial support from the National Natural Science Foundation of China (31101370) and Research and Innovation Initiatives of WHPU (2018Y08).

References

1. R. K. B. Karlsson and A. Cornell, *Chem. Rev.*, 116 (2016) 2982-3028.
2. S. W. Wang, H. L. Xu, P. D. Yao and X. M. Chen, *Electrochemistry*, 80 (2012) 507-511.
3. R. Ming, Y. Zhu, L. Deng, A. Zhang, J. Wang, Y. Han, B. Chai and Z. Ren, *New J. Chem.*, 42

- (2018) 12143-12151.
4. L. Deng, Y. Liu, G. Zhao, J. Chen, S. He, Y. Zhu, B. Chai and Z. Ren, *J. Electroanal. Chem.*, 832 (2019) 459-466.
 5. R. E. Palma-Goyes, J. Vazquez-Arenas, C. Ostos, F. Ferraro, R. A. Torres-Palma and I. Gonzalez, *Electrochim. Acta*, 213 (2016) 740-751.
 6. N. Gedam, N. R. Neti, M. Kormunda, J. Subrt and S. Bakardjieva, *Electrochim. Acta.*, 169 (2015) 109-116.
 7. D. Rajkumar and J. G. Kim, *J. Hazard. Mater.*, 136 (2006) 203-212.
 8. K. Cho, D. Kwon and M. R. Hoffmann, *RSC Adv.*, 4 (2014) 4596-4608.
 9. V. V. Panić, A. Dekanski, S. K. Milonjić, R. T. Atanasoski and B. Ž. Nikolic, *Colloid. Surface. A*, 157 (1999) 269-274.
 10. V. V. Panić, A. Dekanski, S. K. Milonjić, R. T. Atanasoski and B. Ž. Nikolić, *Electrochim. Acta*, 46 (2000) 415-421.
 11. S. Ferro and A. D. Battisti, *J. Phys. Chem. B*, 106 (2002) 2249-2254.
 12. S. Trasatti, *Electrochim. Acta*, 45 (2000) 2377-2385.
 13. S. Trasatti, *Electrochim. Acta*, 29 (1984) 1503-1512.
 14. S. Trasatti, *Electrochim. Acta*, 32 (1987) 369-382.
 15. E. Guerrini, V. Consonni and S. Trasatti, *J. Solid State Electrochem.*, 9 (2005) 320-329.
 16. T. L. Luu, J. Kim and J. Yoon, *J. Ind. Eng. Chem.*, 21 (2015) 400-404.
 17. M. Jiang, H. Wang, Y. Li, H. Zhang, G. Zhang, Z. Lu, X. Sun and L. Jiang, *Small*, 13 (2017) 1602240.
 18. V. Trieu, B. Schley, H. Natter, J. Kintrup, A. Bulan and R. Hempelmann, *Electrochim. Acta*, 78 (2012) 188-194.
 19. C. E. Finke, S. T. Omelchenko, J. T. Jasper, M. F. Lichterman, C. G. Read, N. S. Lewis and M. R. Hoffmann, *Energy Environ. Sci.*, 12 (2018) 4-11.
 20. R. Chen, V. Trieu, H. Natter, K. Stöwe, W. F. Maier, R. Hempelmann, A. Bulan, J. Kintrup and R. Weber, *Chem. Mater.*, 22 (2010) 6215-6217.
 21. M. H. P. Santana, L. M. D. Silva and L. A. D. Faria, *Electrochim. Acta*, 48 (2003) 1885-1891.
 22. J. Kim, C. Kim, S. Kim and J. Yoon, *J. Ind. Eng. Chem.*, 66 (2018) 478-483.
 23. T. Arikawa, Y. Murakami and Y. Takasu, *J. Appl. Electrochem.*, 28 (1998) 511-516.
 24. N. Menzel, E. Ortel, K. Mette, R. Kraehnert and P. Strasser, *ACS Catal.*, 3 (2013) 1324-1333.
 25. R. Chen, V. Trieu, A. R. Zeradjanin, H. Natter, D. Teschner, J. Kintrup, A. Bulan, W. Schuhmann and R. Hempelmann, *Phys. Chem. Chem. Phys.*, 14 (2012) 7392-7399.
 26. H. Cao, D. Lu, J. Lin, Q. Ye, J. Wu and G. Zheng, *Electrochim. Acta*, 91 (2013) 234-239.
 27. K. Macounová, M. Makarova, J. Jirkovský, J. Franc and P. Krtil, *Electrochim. Acta*, 53 (2008) 6126-6134.
 28. Z. Ren, S. Quan, J. Gao, W. Li, Y. Zhu, Y. Liu, B. Chai and Y. Wang, *RSC Adv.*, 5 (2015) 8778-8786.
 29. D. Rosestolato, J. Fregoni, S. Ferro and A. D. Battisti, *Electrochim. Acta*, 139 (2014) 180-189.
 30. A. R. Zeradjanin, N. Menzel, W. Schuhmann and P. Strasser, *Phys. Chem. Chem. Phys.*, 16 (2014) 13741-13747.
 31. L. Vazquez-Gomez, S. Ferro and A. D. Battisti, *Appl. Catal. B: Environ.*, 67 (2006) 34-40.
 32. M. H. P. Santana and L. A. D. Faria, *Electrochim. Acta*, 51 (2006) 3578-3585.
 33. K. S. Exner, J. Anton, T. Jacob and H. Over, *Angew. Chem.*, 128 (2016) 7627-7630.
 34. X.-H. Hu, J.-C. Pan, D. Wang, W. Zhong, H.-Y. Wang and L.-Y. Wang, *Chinese Chem. Lett.*, 26 (2015) 595-598.
 35. R. K. B. Karlsson, H. A. Hansen, T. Bligaard, A. Cornell and L. G. M. Pettersson, *Electrochim. Acta*, 146 (2014) 733-740.
 36. I. Sohrabnejad-Eskan, A. Goryachev, K. S. Exner, L. A. Kibler, E. J. M. Hensen, J. P. Hofmann and H. Over, *ACS Catal.*, 7 (2017) 2403-2411.

37. K. S. Exner, J. Anton, T. Jacob and H. Over, *Angew. Chem. Int. Ed.*, 53 (2014) 11032-11035.
38. H. A. Hansen, I. C. Man, F. Studt, F. Abild-Pedersen, T. Bligaard and J. Rossmeisl, *Phys. Chem. Chem. Phys.*, 12 (2010) 283-290.
39. R. Chen, V. Trieu, H. Natter, J. Kintrop, A. Bulan and R. Hempelmann, *Electrochem. Commun.*, 22 (2012) 16–20.
40. A. R. Zeradjanin, T. Schilling, S. Seisel, M. Bron and W. Schuhmann, *Anal. Chem.*, 83 (2011) 7645-7650.
41. Z. Lu, Y. Li, X. Lei, J. Liu and X. Sun, *Mater. Horiz.*, 2 (2015) 294-298.
42. R. Bavand, A. Yelon and E. Sacher, *Appl. Surf. Sci.*, 355 (2015) 279-289.
43. R. E. Palma-Goyes, J. Vazquez-Arenas, I. C. Romero-Ibarra, C. Ostos, *ChemistrySelect*, 3 (2018) 12937-12945.

© 2019 The Authors. Published by ESG (www.electrochemsci.org). This article is an open access article distributed under the terms and conditions of the Creative Commons Attribution license (<http://creativecommons.org/licenses/by/4.0/>).